Applications of time-resolved photoluminescence for characterizing silicon photovoltaic materials

Zhuofeng Li*⬤**, AnYao Liu, Rabin Basnet, Lachlan E Black, Daniel Macdonald*** **and Hieu T Nguyen**

School of Engineering, The Australian National University, Canberra 2601, Australia

E-mail: zhuofeng.Li@anu.edu.au and daniel.macdonald@anu.edu.au

Abstract

Heavily-doped, amorphous and polycrystalline silicon (poly-Si) layers play important roles in silicon solar cell fabrication and performance. Here we demonstrate applications of time-resolved photoluminescence decay to measure recombination lifetimes in such regions, which are generally below 1 μs, and difficult to measure with other techniques. Firstly, we demonstrate the measurement of Auger lifetimes in uniformly heavily-doped silicon wafers, and show the impact of surface recombination in samples with phosphorus or boron doping concentrations below 1×10^{19} cm^{-3}. We also assess the possible impact of high concentrations of iron contamination on the extraction of such Auger lifetimes. We then report recombination lifetimes measured in thin deposited intrinsic amorphous silicon films, and heavily-doped poly-Si films, as commonly used in passivating contact structures. Interestingly, recombination lifetimes in intrinsic amorphous silicon films can be significantly enhanced by a hydrogenation process. By contrast, recombination lifetimes in heavily-doped poly-Si films vary with different doping profiles for samples fabricated with different deposition techniques, but are not improved by hydrogenation.

Keywords: time-resolved photoluminescence, lifetime, heavily-doped silicon, amorphous silicon, doped polycrystalline silicon, surface passivation

1. Introduction

Heavily-doped regions and deposited silicon (Si) films are fundamental to photovoltaic (PV) technology. These may be present as dopant-diffused regions [1], heavily-doped poly-crystalline silicon (poly-Si) films [2–5], or deposited amorphous silicon (a-Si) layers [6–8]. Recombination lifetimes in these regions and films are generally short (less than 1 μs), due to the heavy doping or defective nature of the materials. One of the most widely used lifetime measurement tools is quasi-steady-state photoconductance (QSSPC) [9], but it is not commonly used to measure ns-scale lifetimes or distinguish the lifetime in the deposited films from a multilayer structure. Microwave photoconductance can be employed to measure short bulk lifetimes in heavily-doped Si [10], but it cannot directly isolate the lifetime in individual layers for structures including perovskite-Si tandem devices, poly-Si passivating contacts and heterojunction solar cells based on a-Si. Lifetime measurements on perovskite materials often employ time-resolved photoluminescence (TRPL) [11, 12].

In this work, TRPL is a suitable technique for measuring lifetimes in both heavily-doped Si and deposited Si

films. We firstly report recombination lifetimes in uniformly heavily-doped Si wafers, which has been previously utilized to measure Auger lifetimes in Si [13–19]. In unpassivated Si wafers, the high surface recombination velocity can result in a time-resolved carrier decay that contains fast and slow decay modes due to surface and bulk components [20]. In this study, we apply surface passivation to heavily-doped Si wafers to eliminate or reduce the initial fast decay lifetime component attributed to surface recombination, allowing accurate determination of the slow decay component due to bulk Auger recombination. This method offers insights to assist reassessment of previous Auger measurements. We also assess the potential impact of iron (Fe) contamination on the determination of Auger lifetimes in heavily-doped Si [21, 22].

Secondly, we measure recombination lifetimes in deposited Si and heavily-doped poly-Si films. TRPL equipped with a short excitation wavelength laser, which is strongly absorbed in these thin layers, is utilized to measure lifetimes at different stages of the fabrication process of Si-based passivating contacts. Hydrogenation is well established as a passivation treatment for deposited Si films, by neutralizing dangling bonds at interfaces and within the bulk [1, 5, 23, 24]. Here we study recombination lifetimes within intrinsic a-Si films, and their response to hydrogenation. Such films are an essential component of Si heterojunction solar cell technology [6, 8]. We also deposit intrinsic a-Si or poly-Si films on a SiO_x/c-Si structure, which are the precursors to form doped poly-Si passivating contacts, commonly used in the PV industry today in so-called TOPCon [2, 3] or POLO cells [5]. By performing annealing and hydrogenation on these precursors, we study changes in the recombination lifetimes within these films. In addition, we employ a high-temperature *ex-situ* dopant diffusion process to these deposited Si precursors to form phosphorus-doped poly-Si electron-selective contacts [4, 23]. We use TRPL to examine the lifetimes in these heavily-doped poly-Si contacts, and observe the impact of hydrogenation.

2. Experimental details

The TRPL measurement results in a time-resolved transient decay courtesy of single photon counting under a pulsed laser excitation source. A pulsed laser diode (Horiba DeltaDiode) is focused on the sample through a 50X objective lens, with a laser spot size of 10 μm in diameter. The PL signal emitted from the same side of the sample is captured by a Horiba iHR 320 mm spectrophotometer equipped with a thermoelectric cooled InGaAs photomultiplier tube with a detection range between 950 nm and 1700 nm. The pulsed laser frequencies can be varied from 100 kHz to 25 MHz. Two different pulsed excitation lasers are employed in the TRPL measurements, with peak excitation wavelengths at 485 nm and 785 nm, and short pulse widths at 80 ps and 60 ps, respectively. The on-sample power of the 485 nm laser is 23.5 μW, and 1.85 μW for the 785 nm laser, which yields an estimated excess carrier concentration on the order of 10^{14}–10^{15} cm^{-3}. Two experimental TRPL configurations were used in this study. For

uniformly heavily-doped Si wafers, room-temperature TRPL measurements at 300 K were conducted with an excitation wavelength at 785 nm. Low-temperature measurements at 80 K were employed for deposited Si and heavily-doped poly-Si films with an excitation wavelength at 485 nm. An as-cut Cz phosphorus-doped Si wafer with 2 Ω cm resistivity was used to estimate the system response. The as-cut surface results in very rapid recombination when using the strongly absorbed excitation wavelength of 485 nm. This allowed us to estimate an upper limit of the characteristic system response time, in order to exclude its impact on recombination lifetime measurements.

The first set of samples were single-side polished Cz heavily-doped Si wafers with phosphorus (n$^+$) and boron (p$^+$) doping concentrations from 2.9 $\times$ 10^{18} cm^{-3} to 1.1 $\times$ 10^{20} cm^{-3}. These wafers were chosen for the study of Auger lifetimes. After etching in a tetramethylammonium hydroxide (TMAH) solution, the doping densities were acquired by an electrochemical capacitance-voltage (ECV) profiling method [4], in which the etched area was measured by an optical microscope. The highest doping densities were 6.5 $\times$ 10^{19} cm^{-3} for n$^+$ and 1.1 $\times$ 10^{20} cm^{-3} for p$^+$ Si, with a thickness of 300 $\pm$ 10 μm. The other wafers had a thickness of 500 $\pm$ 10 μm. Dilute hydrofluoric acid (HF) was used to remove the residual oxide on the surface before TRPL measurements. After a standard RCA cleaning process, some n$^+$ Si wafers were coated with 80 nm thick hydrogenated SiN$_x$:H films via plasma enhanced chemical vapour deposition (PECVD) [25], while some p$^+$ Si wafers were deposited with 60 nm thick hydrogenated Al$_2$O$_3$ using plasma assisted atomic layer deposition (PAALD) [26]. The surface passivation effect was activated by a subsequent annealing in forming gas (5% H$_2$, 95% Ar) at 425 °C for 30 min [4, 23]. Note that these capping layers were retained during TRPL measurements. We performed the measurements on both the unpolished and polished sides and observed no significant difference in the lifetime result.

In addition, we investigated the impact of intentional Fe contamination on the recombination lifetime in these heavily-doped wafers, since in practical solar cells, such heavily doped regions often act as gettering sinks for metal contamination [22, 27]. In this case, the doping densities of the heavily-doped Si wafer bulk were 6.5 $\times$ 10^{19} cm^{-3} for n$^+$ and 1.1 $\times$ 10^{20} cm^{-3} for p$^+$ Si. Fe contamination was carried out by ion implantation of ^{56}Fe, followed by a thermal annealing process at 1050 °C for 3 h to distribute the interstitial Fe contaminants evenly across the sample thickness of 300 μm. The first 1.5 h annealing was carried out in dry O$_2$ ambient, and then 1.5 h in N$_2$. A ramp-down process of 10 °C min^{-1} in N$_2$ was then applied, and the samples were unloaded from the furnace at 900 °C, before cooling in high air flow to reach room temperature within a few minutes. We then used a TMAH solution to remove any residual ion implantation related surface damage after annealing. A set of control samples without Fe contamination also underwent the same annealing and etching processes.

After distributing the implanted Fe atoms throughout the wafer thickness, bulk Fe concentrations of 1 $\times$ 10^{15} cm^{-3} for

the p$^+$ sample, and 1×10^{15} cm^{-3} and 1×10^{16} cm^{-3} for the n$^+$ Si samples, were expected. The solubility limit of Fe at 1050 °C in intrinsic Si is 1×10^{15} cm^{-3} [28]. At the unloading temperature of 900 °C, the Fe solubility in intrinsic Si is 4×10^{13} cm^{-3} [28]. However, in heavily-doped Si, the apparent Fe solubility is enhanced by a factor termed the segregation coefficient. For the n$^+$ Si with a phosphorus doping of 6.5×10^{19} cm^{-3}, the reported segregation coefficient is 10–310 at 1050 °C and 80–5400 at 900 °C [29, 30], and is ∼2 at 1050 °C and ∼8 at 900 °C for the p$^+$ Si sample if assuming only contributions from electrically active boron dopants [31]. Considering the large range of the reported segregation coefficients, the enhanced Fe solubilities are likely close to, or exceed, the target Fe concentrations, meaning that Fe precipitation is insignificant. In addition, a very rapid cooldown from 900 °C was applied. Our previous studies, which performed similar thermal annealing processes, consistently found negligible amount of Fe precipitation [27, 32]. Note that the exact state of Fe in heavily-doped Si is not entirely clear, as there are different hypotheses to explain the apparent enhanced Fe solubility [22]. Nevertheless, this does not affect the interpretation of our results. Since we cannot entirely exclude the possibility of Fe precipitation to wafer surfaces, the intended Fe concentrations of 1×10^{15} cm^{-3} for the p$^+$, and 1×10^{15} cm^{-3} and 1×10^{16} cm^{-3} for the n$^+$ Si samples are regarded as the upper limits of the Fe concentrations.

Secondly, we investigated the recombination lifetimes in deposited Si films. Cz phosphorus-doped Si wafers were chosen, with 2 Ω cm resistivity and 250 ± 5 μm thickness after etching in a TMAH solution to remove the saw damage. The wafers underwent a standard RCA cleaning before a thermal oxidation process at 600 °C in O$_2$ ambient for 5 min [4]. Some samples were coated with hydrogenated PECVD a-Si:H of ∼40 nm [4, 23], while some samples were deposited with ∼80 nm intrinsic poly-Si using a low-pressure chemical vapour deposition (LPCVD) technique [5]. The as-deposited PECVD a-Si:H underwent a thermal annealing at 600 °C in N$_2$ ambient for 30 min to remove the hydrogen content in the film [23, 33]. These annealed films are referred to here as intrinsic deposited Si. Both PECVD and LPCVD intrinsic deposited Si samples went through a hydrogenation treatment via PECVD SiN$_x$:H and a subsequent annealing in forming gas at 425 °C for 30 min. In addition, some as-deposited PECVD a-Si:H and LPCVD poly-Si samples were used as precursors to fabricate doped poly-Si contact structures. We employed an *ex-situ* POCl$_3$ diffusion at 830 °C, with 25 min dopant deposition and then 25 min drive-in annealing in N$_2$ ambient [4, 23]. The phosphorus silicate glass layers were removed by a dilute HF solution. The doping concentrations in the heavily-doped poly-Si films were assessed by ECV profiling. Some of these samples were also subject to hydrogenation with PECVD SiN$_x$:H and forming gas annealing.

For both deposited Si and heavily-doped poly-Si films in this study, the hydrogenated dielectric films were removed by a dilute HF dip. Steady-state PL spectra were then measured with a Horiba iHR 320 mm confocal micro-PL system at 80 K, with a temperature controlled THMS600 Linkam stage. These spectra were consistent with PL signatures for deposited Si

and doped poly-Si films, as previously reported [23, 34]. The hydrogenation effect on wafer surface passivation provided by the doped poly-Si films was also assessed by transient and QSSPC measurements using a Sinton Instruments WCT-120 photoconductance tester, to determine the implied open circuit voltage (iV$_{OC}$) [9]. For low-temperature TRPL measurements, the transient decays of PL emission from the doped poly-Si regions were measured using a long-pass filter with a cut-off wavelength at 1250 nm to eliminate the component from the band-to-band PL of the c-Si substrate.

3. Results and discussion

3.1. Auger lifetimes in uniformly heavily-doped Si wafers

Figure 1 shows the normalized PL decays of several unpassivated samples after a dilute HF dip. A simple derivation of the effective lifetime is realized by extracting the time constant of the exponential decay curves. In general, the Si bulk lifetime can be affected by multiple recombination channels including radiative recombination [35], Shockley-Read-Hall (SRH) recombination through defects [36], and Auger recombination. At high doping or injection levels, Auger recombination is often dominant. Under high injection, the Auger lifetime is strongly dependent on the illumination intensity, due to its quadratic dependence on the excess carrier concentration [37, 38]. However, as shown for each of the heavily-doped Si wafers in figure 1, the normalized TRPL decay curves are unchanged with different illumination intensities, although an increasing noise level is associated with a reduced excitation power. This demonstrates that these samples are under low injection conditions, as expected due to their very high doping concentrations. As such, the Auger lifetime depends only on the sample doping density, and not the illumination intensity [37, 38].

At very high doping levels over 2.5×10^{19} cm^{-3} shown in figures 1(a) and (b), only one time constant is present in the normalized decay, from which we extract the effective lifetime with a single exponential decay fit. However, curved decays occur in both figures 1(c) and (d), which complicates the extraction of the effective lifetime. A similar two-time-constant decay was observed in the early Auger lifetime study by Dziewior and Schmid on an n$^+$ sample with a doping concentration of 9.7×10^{18} cm^{-3} [14]. The fast decay component was attributed to surface recombination, and the slow decay component was reported as the bulk Auger lifetime. Luke and Cheng presented a quantitative analysis to study the separation of the fast and slow decay modes, which has been widely adapted in transient analysis to understand the relationship between the surface recombination velocity and bulk minority carrier lifetime [20].

In order to confirm that the fast decay mode is caused by surface recombination, we performed TRPL measurements on samples with surface passivating films—SiN$_x$:H films on n$^+$ wafers, with positive fixed charges to repel minority holes, and Al$_2$O$_3$ films on p$^+$ wafers, with negative fixed charges to repel minority electrons. TRPL measurements on surface passivated samples with doping densities exceeding 2.5×10^{19} cm^{-3}
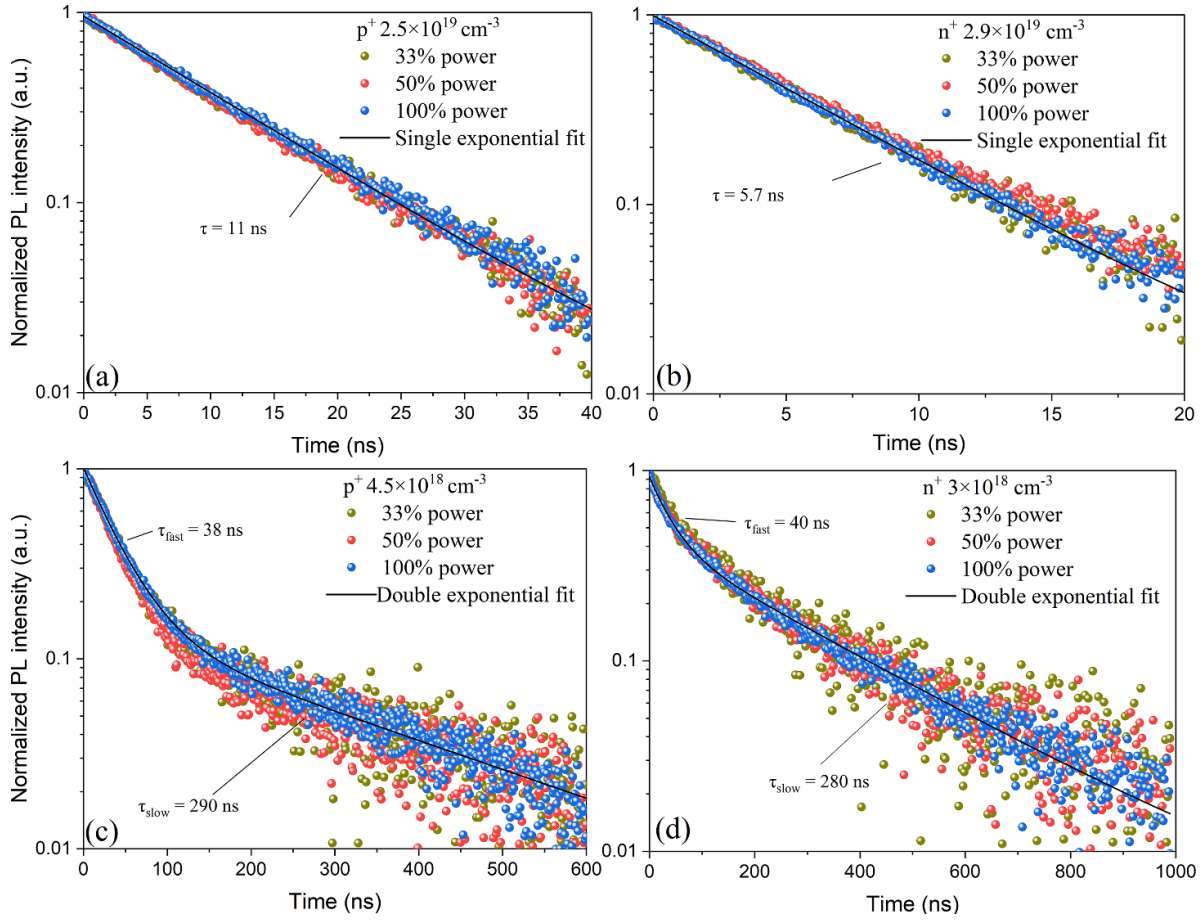
Figure 1. Normalized TRPL decays of four unpassivated heavily-doped Si samples. Each sample is measured with varying illumination intensities. (a) and (b): Only one time constant can be observed in the decay curves. A single exponential decay fit is used to extract the Auger lifetime. (c) and (d): Two time constants can be observed in the decay curves. A double exponential decay fit is used. Lifetimes are extracted with the fast decay mode attributed to surface recombination, and the slow decay mode representing the bulk lifetime dominated by Auger recombination.

revealed no significant impact on the decay curves. For doping densities under 1×10^{19} cm^{-3}, the fast decay mode due to surface recombination is eliminated or reduced by the surface passivation treatment, as shown in figure 2. For the n$^+$ sample in figure 2(b), the decay time for the passivated sample is similar to the second time constant for the unpassivated sample, meaning it can be reasonably attributed to bulk Auger recombination. However, for the p$^+$ sample in figure 2(a), the time constant for the passivated sample is still shorter than the second time constant for the unpassivated sample. This indicates that the surface passivation is imperfect in this case, and still impedes the extraction of the Auger lifetime. Generally, we found that p$^+$ Si wafers were more difficult to achieve sufficient surface passivation on than n$^+$ Si wafers.

Nevertheless, with surface passivation films present, we extract the apparent Auger lifetimes from single-exponential decay fits and present these results in figures 3(a) and (b), compared to earlier measurement data [13–19], together with the slow decay lifetimes in unpassivated samples in this work. Note that the data presented by Dziewior and Schmid [14] was revised by Black and Macdonald [39] by adopting a more recent mobility model to estimate the doping densities.

Auger lifetimes in both unpassivated and passivated n$^+$ Si wafers in this study agree well with previous research, particularly the data of del Alamo *et al* [15] and Swirhun *et al* [17] at higher doping densities and the data of Häcker and Hangleiter [19] at lower densities, whereas the Auger lifetimes in p$^+$ Si show agreement with different published results depending on whether they were obtained from passivated or unpassivated samples. Our p$^+$ Si lifetimes in the passivated samples agree with the data presented by Swirhun *et al* [16], and both give shorter Auger lifetimes for doping densities within the range from 1×10^{18} cm^{-3}–1×10^{19} cm^{-3} in comparison to other studies. Swirhun *et al* used an excitation wavelength of 647 nm, similar to our 785 nm laser, and their samples were subject to thermal oxidation which could also have an impact on the surface recombination [18]. Other studies used either longer wavelengths above 1000 nm, in which case surface recombination was less significant, or used shorter wavelengths, but with more sensitive detection which allows the slow decay component to be measured accurately. Consistent with this, we note that our p$^+$ Si lifetimes extracted from the slow decays of the unpassivated samples agree well with the other Auger lifetime studies. We conclude that the
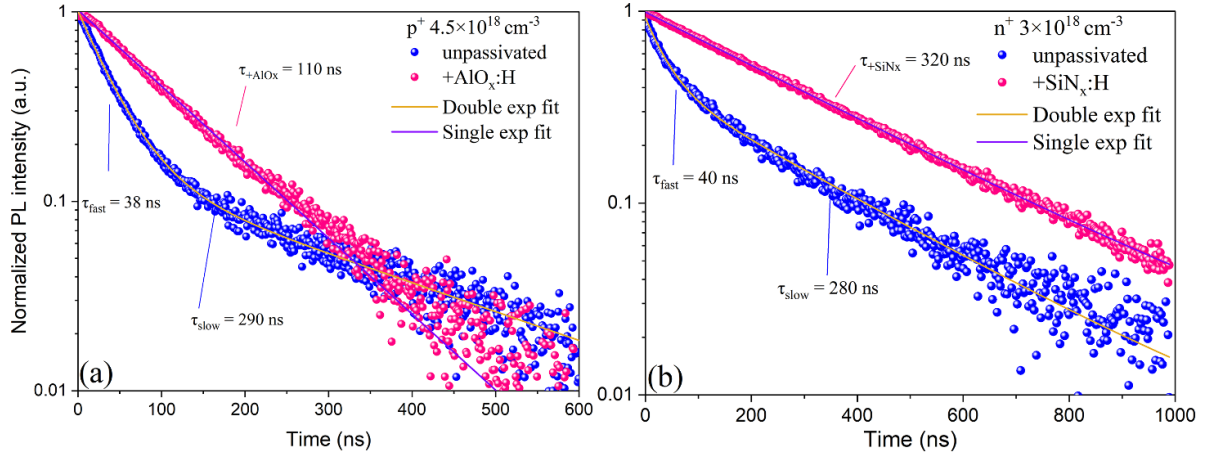
Figure 2. TRPL decay comparison between unpassivated and passivated heavily-doped Si of (a) p^+ samples, and (b) n^+ samples. The decays of the unpassivated samples are fitted using a double exponential fit, whereas the decays with surface passivation are fitted using a single exponential fit.
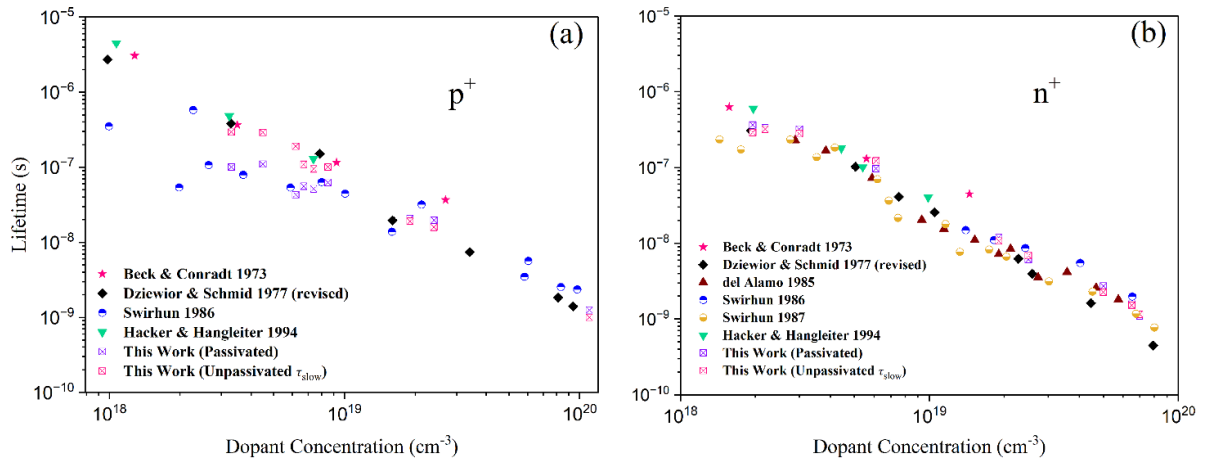

Figure 3. (a) and (b): Auger lifetimes in p^+ and n^+ Si at doping levels over 1×10^{18} cm^{-3}.

discrepancy in the passivated samples is caused by imperfect surface passivation from the Al_2O_3 films used in this work.

Fe contamination of heavily doped regions, as occurs during gettering of Si solar cells [22, 27], can introduce additional recombination centers in the heavily-doped Si layers [40]. Here we study the possible impact of such metallic contamination on the bulk lifetimes in heavily-doped Si wafers. The TRPL decay curves of Fe-implanted heavily-doped samples are shown in figure 4. Note that these wafers with high doping densities do not require surface passivation. Both the control and Fe-contaminated samples underwent the same annealing treatment and a subsequent TMAH etching process. The identical carrier decay curves, despite Fe contamination, suggest the lifetimes in these wafers are not affected by Fe-induced defect states with upper limits of volumetric concentrations of 1×10^{15} cm^{-3} for p^+ Si, 1×10^{15} cm^{-3} and 1×10^{16} cm^{-3} for n^+ Si. These Fe doses correspond to Fe concentrations on the order of 10^{12}–10^{13} cm^{-3} in the bulk of a 130-μm thick Si wafer, if gettered to a thin p^+ or n^+ region near the surface. We conclude that Auger recombination is still

entirely dominant in these heavily-doped Si samples for p^+ Si of 1.1×10^{20} cm^{-3} and n^+ Si of 6.5×10^{19} cm^{-3}, regardless of the applied high Fe concentrations. This finding does not contradict other studies where the investigated p^+ concentrations were lower and thus SRH recombination due to Fe became more noticeable [40, 41].

3.2. Lifetimes in intrinsic deposited Si films

Steady-state PL spectra of deposited Si films, measured using the confocal micro-PL system at 80 K, are shown in figure 5(a). The as-deposited PECVD hydrogenated a-Si:H films emit strong PL intensities with a peak between 900 to 1000 nm. After a thermal annealing process at 600 °C, the films show negligible PL emission, due to defect states activated by hydrogen effusion, as reported previously [23, 33]. This response indicates that the high PL intensity emitted from the as-deposited Si films denotes the presence of hydrogen, and the passivation of defect states within the films.
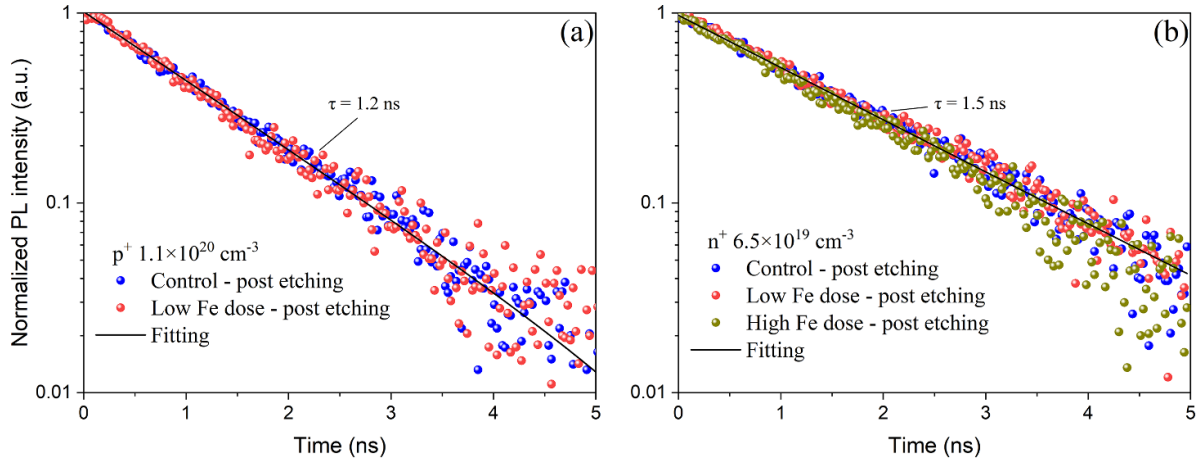
Figure 4. TRPL decay curves of (a) p^+ Si and (b) n^+ Si subject to Fe contamination. The lifetimes are extracted with a single exponential decay fit. A low Fe dose corresponds to an upper limit of Fe contamination of $1 \times 10^{15} cm^{-3}$, and a high Fe dose corresponds to an upper limit of $1 \times 10^{16} cm^{-3}$.
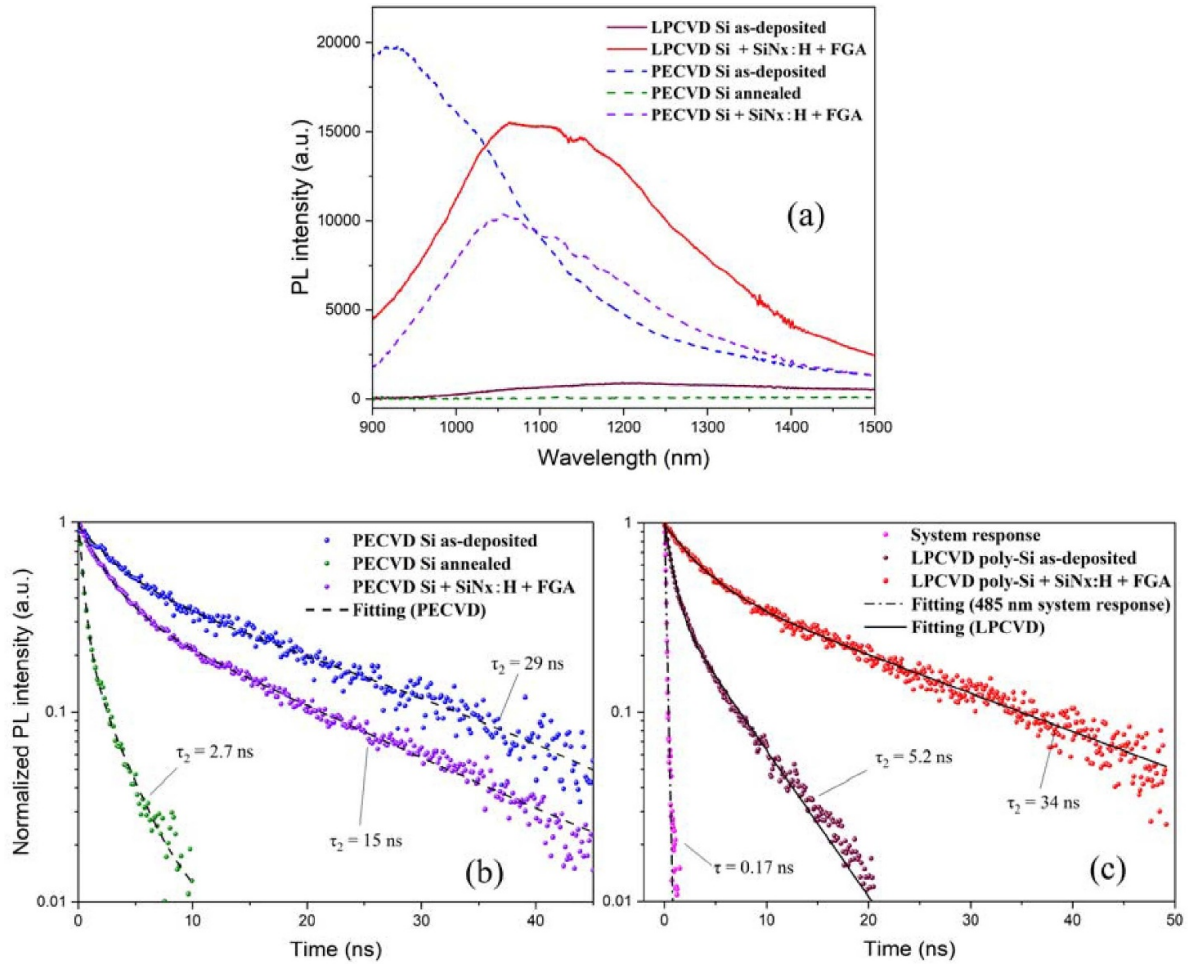

Figure 5. (a) Steady-state PL spectra of PECVD and LPCVD deposited Si films, measured by an excitation wavelength at 405 nm. (b) TRPL decay curves of PECVD deposited Si, measured by an excitation wavelength at 485 nm. (c) TRPL decay curves of LPCVD deposited Si. An as-cut Si wafer of 2 Ω cm is used to estimate an upper limit for the system response time.

The annealed deposited Si films were then subject to surface passivation by hydrogen-rich SiN_x:H films plus forming gas annealing, creating a re-hydrogenation effect. Strong PL spectra can be observed again, emitted from the deposited Si layers, not from the SiN_x:H films which were removed by a dilute HF dip. In figure 5(a), the broad PL peak is shifted
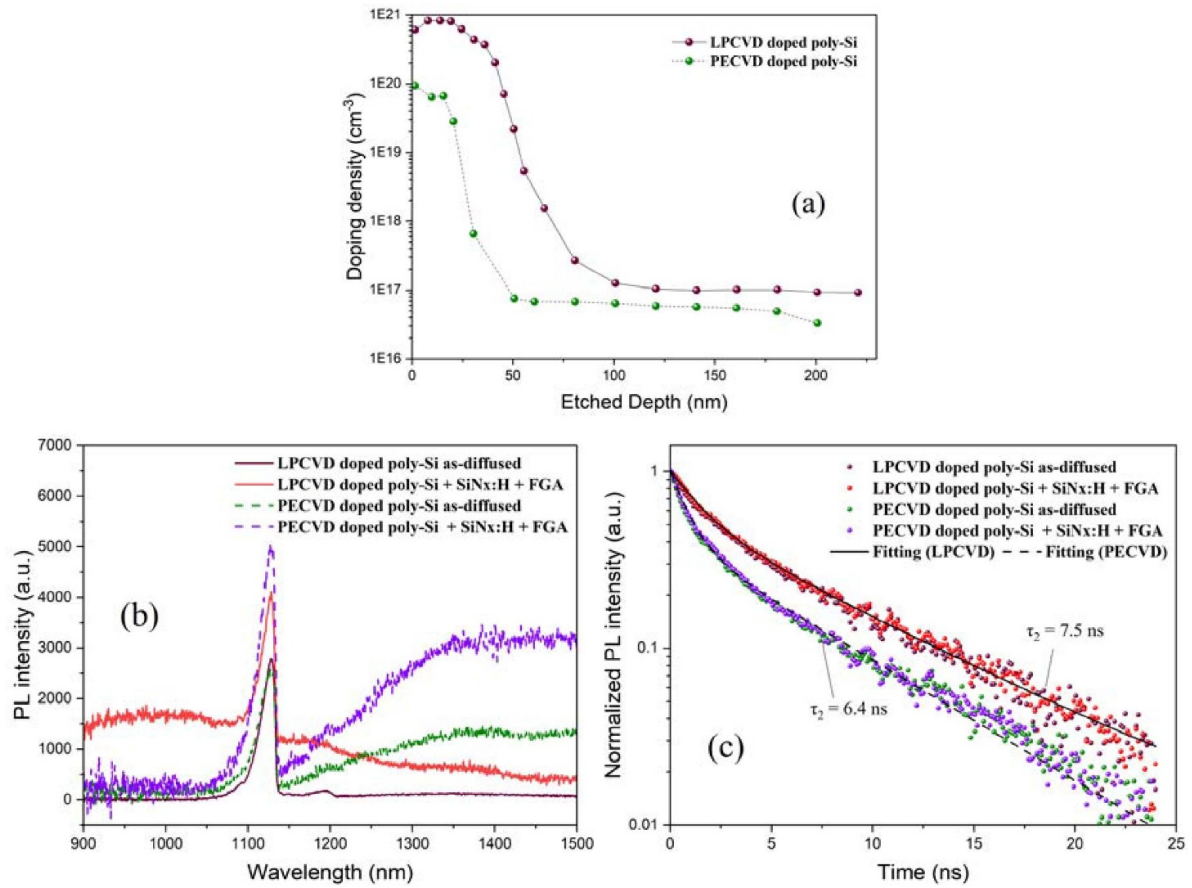
Figure 6. (a) ECV profiles of PECVD and LPCVD phosphorus-doped poly-Si. (b) Steady-state PL spectra of PECVD and LPCVD phosphorus-doped poly-Si, measured by an excitation wavelength at 405 nm. (c) TRPL decay curves of PECVD and LPCVD phosphorus-doped poly-Si, measured by an excitation wavelength at 485 nm.

towards longer wavelengths compared to the as-deposited a-Si:H. This PL shift could reflect partial crystallization of the amorphous phase during thermal annealing at 600 °C [42].

Figures 5(b) and (c) compare the lifetimes within both PECVD and LPCVD deposited Si films by fitting the transient decay curves captured by TRPL at 80 K. We present two lifetime components extracted from the decay curves with a double exponential decay fit. An excitation wavelength at 485 nm was employed in such TRPL measurements. The lifetime measured from the 2 Ω cm Si as-cut wafer with highly defective surface is also displayed in figure 5(c), showing a short decay lifetime of 0.17 ns, which is an upper limit for the system response. Compared to the as-deposited PECVD a-Si:H, the lifetime reduces significantly due to hydrogen effusion during thermal annealing. Re-hydrogenation then gives rise to a lifetime increase again in the PECVD deposited Si films. TRPL measurements on deposited Si were also demonstrated by Wu *et al* who reported the loss of hydrogen in PECVD a-Si:H films during a 400 °C annealing process by showing a lifetime reduction from 2.93 ns to 1.96 ns [43]. This work presents a more significant lifetime change. The as-deposited PECVD a-Si:H lifetime drops from 29 ns to 2.7 ns when residual hydrogen was driven out of the films, and then increases to 15 ns after re-hydrogenation. Similarly, LPCVD deposited Si films exhibit a short minority carrier lifetime of

5.2 ns, but can exceed 30 ns after hydrogenation. In general, the bulk lifetime in intrinsic deposited Si is affected by defect states inside the films, and can be significantly improved by a hydrogenation process.

3.3. Lifetimes in phosphorus-doped poly-Si films

The precursors used for determining the deposited Si lifetime underwent a POCl$_3$ diffusion to form phosphorus-doped poly-Si electron-selective contacts. The ECV results of the doped poly-Si films are shown in figure 6(a), presenting the electrically active phosphorus doping profiles in these films. The LPCVD doped poly-Si films have a higher phosphorus doping profile and a larger thickness of doped poly-Si region. Micro-PL spectra in figure 6(b) depict the band-to-band PL emission from the c-Si substrate at around 1130 nm [23, 34]. The broad PL signatures at longer wavelengths originate from the doped poly-Si films [23]. We present the increase in PL intensities when the defect states were passivated by PECVD SiN$_x$:H hydrogenation. In addition, QSSPC measurements show an increase in iV$_{OC}$ due to hydrogenation from 682 mV to 703 mV for PECVD doped poly-Si, and from 693 mV to 710 mV for LPCVD doped poly-Si. Both micro-PL and QSSPC measurements indicate an effective hydrogenation improvement for the doped poly-Si films.

In figure 6(c), a double exponential decay fitting is employed where the first time constant is assumed to originate from the system response and surface recombination. The second exponential decay component is regarded as the bulk lifetime in the doped poly-Si films. Doped poly-Si fabricated from different deposition techniques yield different lifetimes. These lifetimes in heavily-doped poly-Si films remain unchanged regardless of hydrogenation, which implies that defect passivation does not have a measurable impact on the bulk lifetime in such films. This may suggest that Auger recombination is dominant in the bulk of the heavily-doped poly-Si layers.

4. Conclusions

In summary, this paper demonstrates some applications of TRPL to measure carrier lifetimes in various Si materials with recombination lifetimes below 1 μs. Auger lifetimes can be extracted from low-injection TRPL measurements on heavily-doped Si wafers, subject to consideration of surface recombination for doping concentrations below 1×10^{19} cm^{-3} when using an illumination wavelength of 785 nm. This study also reveals that Fe-induced recombination centers do not noticeably affect the bulk lifetime in either heavily phosphorus- (6.5×10^{19} cm^{-3}) or boron- (1.1×10^{20} cm^{-3}) doped Si for the conditions investigated in this study. Additionally, low-temperature TRPL measurements are demonstrated for intrinsic deposited Si and heavily-doped poly-Si films processed with hydrogenation treatments. Hydrogenation effectively increases the recombination lifetime in intrinsic deposited Si films. By contrast, hydrogenation does not improve the recombination lifetime in heavily-doped poly-Si films, despite hydrogenation improving the surface passivation of the contact itself, as evidenced by increased iV$_{OC}$ values. This work also reveals differences in the recombination lifetime in heavily-doped poly-Si films fabricated with different deposition techniques with varying doping concentration profiles.

Data availability statement

The data that support the findings of this study are available upon reasonable request from the authors.

Acknowledgment

Conflict of interest

The authors declare that there are no conflicts of interest related to this work.

Ethics statement

This study does not involve human participants, animals, or any procedures requiring ethical approval.

ORCID iD

Zhuofeng Li ⓘ https://orcid.org/0009-0000-0028-753X

References

[1] Feldmann F, Schön J, Niess J, Lerch W and Hermle M 2019 Studying dopant diffusion from Poly-Si passivating contacts *Sol. Energy Mater. Sol. Cells* **200** 109978

[2] Feldmann F, Bivour M, Reichel C, Hermle M and Glunz S W 2014 Passivated rear contacts for high-efficiency n-type Si solar cells providing high interface passivation quality and excellent transport characteristics *Sol. Energy Mater. Sol. Cells* **120** 270–4

[3] Feldmann F, Bivour M, Reichel C, Steinkemper H, Hermle M and Glunz S W 2014 Tunnel oxide passivated contacts as an alternative to partial rear contacts *Sol. Energy Mater. Sol. Cells* **131** 46–50

[4] Yan D, Cuevas A, Bullock J, Wan Y and Samundsett C 2015 Phosphorus-diffused polysilicon contacts for solar cells *Sol. Energy Mater. Sol. Cells* **142** 75–82

[5] Haase F, Hollemann C, Schäfer S, Merkle A, Rienäcker M, Krügener J, Brendel R and Peibst R 2018 Laser contact openings for local poly-Si-metal contacts enabling 26.1%-efficient POLO-IBC solar cells *Sol. Energy Mater. Sol. Cells* **186** 184–93

[6] Taguchi M, Yano A, Tohoda S, Matsuyama K, Nakamura Y, Nishiwaki T, Fujita K and Maruyama E 2014 24.7% Record efficiency HIT solar cell on thin silicon wafer *IEEE J. Photovolt.* **4** 96–99

[7] Matsui T *et al* 2015 High-efficiency amorphous silicon solar cells: impact of deposition rate on metastability *Appl. Phys. Lett.* **106** 053901

[8] Ru X, Qu M, Wang J, Ruan T, Yang M, Peng F, Long W, Zheng K, Yan H and Xu X 2020 25.11% efficiency silicon heterojunction solar cell with low deposition rate intrinsic amorphous silicon buffer layers *Sol. Energy Mater. Sol. Cells* **215** 110643

[9] Sinton R A and Cuevas A 1996 Contactless determination of current–voltage characteristics and minority-carrier lifetimes in semiconductors from quasi-steady-state photoconductance data *Appl. Phys. Lett.* **69** 2510–2

[10] Gyüre-Garami B, Blum B, Sági O, Bojtor A, Kollarics S, Cssz G, Márkus B G, Volk J and Simon F 2019 Ultrafast sensing of photoconductivity decay using microwave resonators *J. Appl. Phys.* **126** 235702

[11] Dewi H A *et al* 2019 Highly efficient semitransparent perovskite solar cells for four terminal perovskite-silicon tandems *ACS Appl. Mater. Interfaces* **11** 34178–87

[12] Péan E V, Dimitrov S, De Castro C S and Davies M L 2020 Interpreting time-resolved photoluminescence of perovskite materials *Phys. Chem. Chem. Phys.* **22** 28345–58

[13] Beck J D and Conradt R 1973 Auger-rekombination in Si *Solid State Commun.* **13** 93–95

[14] Dziewior J and Schmid W 1977 Auger coefficients for highly doped and highly excited silicon *Appl. Phys. Lett.* **31** 346–8

[15] Del Alamo J, Swirhun S and Swanson R M 1985 Simultaneous measurement of hole lifetime, hole mobility and bandgap narrowing in heavily doped n-type silicon *1985 Int. Electron Devices Meeting* pp 290–3

[16] Swirhun S E, Kwark Y-H and Swanson R M 1986
Measurement of electron lifetime, electron mobility and
band-gap narrowing in heavily doped p-type silicon *1986
Int. Electron Devices Meeting* pp 24–27

[17] Swirhun S, Swanson J A, Del Alamo J A and Swanson R M
1986 Measurement of hole mobility in heavily doped n-type
silicon *IEEE Electron Device Lett.* **7** 168–71

[18] Swirhun S E 1987 *Characterization of Majority and Minority
Carrier Transport in Heavily Doped Silicon* (Stanford
University)

[19] Häcker R and Hangleiter A 1994 Intrinsic upper limits of the
carrier lifetime in silicon *J. Appl. Phys.* **75** 7570–2

[20] Luke K L and Cheng L-J 1987 Analysis of the interaction of a
laser pulse with a silicon wafer: determination of bulk
lifetime and surface recombination velocity *J. Appl. Phys.*
61 2282–93

[21] Myers S M, Seibt M and Schröter W 2000 Mechanisms of
transition-metal gettering in silicon *J. Appl. Phys.*
88 3795–819

[22] Liu A, Phang S P and Macdonald D 2022 Gettering in silicon
photovoltaics: a review *Sol. Energy Mater. Sol. Cells*
234 111447

[23] Truong T N, Yan D, Samundsett C, Basnet R,
Tebyetekerwa M, Li L, Kremer F, Cuevas A, Macdonald D
and Nguyen H T 2019 Hydrogenation of phosphorus-doped
polycrystalline silicon films for passivating contact solar
cells *ACS Appl. Mater. Interfaces* **11** 5554–60

[24] van de Loo B W H, Macco B, Schnabel M, Stodolny M K,
Mewe A A, Young D L, Nemeth W, Stradins P and
Kessels W M M 2020 On the hydrogenation of Poly-Si
passivating contacts by Al_2O_3 and SiN_x thin films *Sol.
Energy Mater. Sol. Cells* **215** 110592

[25] Kerr M J and Cuevas A 2002 Recombination at the interface
between silicon and stoichiometric plasma silicon nitride
Semicond. Sci. Technol. **17** 166

[26] Hoex B, Schmidt J, Bock R, Altermatt P P, Van De
Sanden M C M and Kessels W M M 2007 Excellent
passivation of highly doped p-type Si surfaces by the
negative-charge-dielectric Al_2O_3 *Appl. Phys. Lett.*
91 112107

[27] Liu A, Yan D, Phang S P, Cuevas A and Macdonald D 2018
Effective impurity gettering by phosphorus-and
boron-diffused polysilicon passivating contacts for silicon
solar cells *Sol. Energy Mater. Sol. Cells* **179** 136–41

[28] Istratov A A, Hieslmair H and Weber E R 1999 Iron and its
complexes in silicon *Appl. Phys. A* **69** 13–44

[29] Talvitie H, Vähänissi V, Haarahiltunen A, Yli-Koski M and
Savin H 2011 Phosphorus and boron diffusion gettering of
iron in monocrystalline silicon *J. Appl. Phys.* **109** 093505

[30] Schön J, Vähänissi V, Haarahiltunen A, Schubert M C,
Warta W and Savin H 2014 Main defect reactions behind
phosphorus diffusion gettering of iron *J. Appl. Phys.*
116 244503

[31] McHugo S A, McDonald R J, Smith A R, Hurley D L and
Weber E R 1998 Iron solubility in highly boron-doped
silicon *Appl. Phys. Lett.* **73** 1424–6

[32] Liu A and Macdonald D 2017 Impurity gettering effect of
atomic layer deposited aluminium oxide films on silicon
wafers *Appl. Phys. Lett.* **110** 191604

[33] Budini N, Rinaldi P A, Schmidt J A, Arce R D and
Buitrago R H 2010 Influence of microstructure and
hydrogen concentration on amorphous silicon
crystallization *Thin Solid Films* **518** 5349–54

[34] Nguyen H T *et al* 2018 Sub-bandgap luminescence from
doped polycrystalline and amorphous silicon films and its
application to understanding passivating-contact solar cells
ACS Appl. Energy Mater. **1** 6619–25

[35] Trupke T, Green M A, Würfel P, Altermatt P P, Wang A,
Zhao J and Corkish R 2003 Temperature dependence of the
radiative recombination coefficient of intrinsic crystalline
silicon *J. Appl. Phys.* **94** 4930–7

[36] Shockley W and Read W T Jr 1952 Statistics of the
recombinations of holes and electrons *Phys. Rev.*
87 835–42

[37] Kerr M J and Cuevas A 2002 General parameterization of
Auger recombination in crystalline silicon *J. Appl. Phys.*
91 2473–80

[38] Richter A, Werner F, Cuevas A, Schmidt J and Glunz S W
2012 Improved parameterization of Auger recombination in
silicon *Energy Proc.* **27** 88–94

[39] Black L E and Macdonald D H 2022 On the quantification of
Auger recombination in crystalline silicon *Sol. Energy
Mater. Sol. Cells* **234** 111428

[40] Macdonald D, Mäckel H and Cuevas A 2006 Effect of gettered
iron on recombination in diffused regions of crystalline
silicon wafers *Appl. Phys. Lett.* **88** 092105

[41] Yang Z *et al* 2025 Effect of iron contamination and polysilicon
gettering on the performance of polysilicon-based
passivating contact solar cells *Prog. Photovolt., Res. Appl.*
33 463–76

[42] Lee J N *et al* 1997 Effect of deposition temperature on the
crystallization mechanism of amorphous silicon films on
glass *Jpn. J. Appl. Phys.* **36** 6862

[43] Wu H, Nguyen H T, Black L, Liu A, Liu R, Chen W, Kang D,
Yang W and Macdonald D 2020 A correlative study of film
lifetime, hydrogen content, and surface passivation quality
of amorphous silicon films on silicon wafers *IEEE J.
Photovolt.* **10** 1307–12